Hydrology and
Earth System
Sciences

Open Access

Discussions

Hortonian overland flow closure relations in the Representative Elementary Watershed Framework evaluated with observations

E. Vannametee, D. Karssenberg, M. R. Hendriks, and M. F. P. Bierkens

Department of Physical Geography, Faculty of Geosciences, Utrecht University, P.O. Box 80115, 3508 TC Utrecht, The Netherlands

Correspondence to: E. Vannametee (e.vannametee@uu.nl)

HESSD

10, 1769–1817, 2013

Hortonian overland flow closure relations

E. Vannametee et al.

Title Page

Abstract | Introduction

Conclusions | References

Tables | Figures

◄◄ | ►►

◄ | ►

Back | Close

Full Screen / Esc

Printer-friendly Version

Interactive Discussion

Abstract

This paper presents an evaluation of the closure relation for Hortonian runoff that explicitly accounts for sub-REW process heterogeneity and scale effects, proposed in Vannametee et al. (2012). We apply the closure relation, which is embedded in an
5 event-based rainfall-runoff model developed under the REW framework, to a $15\,km^2$ catchment in the French Alps. The scaling parameters in the closure relation are directly estimated using local and thus observable REW properties and rainstorm characteristics. Evaluation of the simulation results against the observed discharge indicates good performance in reproducing the hydrograph and discharge volume, even
10 without calibration. The discharge prediction exhibits a significant improvement when the closure relation is calibrated with catchment-scale runoff. Our closure relation also yields better predictions when compared with results from a benchmark closure relation that does not consider scale effects. Calibration is done by only changing one of the REW observables, i.e. hydraulic conductivity, as that determines the scaling param-
15 eters, using a single prefactor for the entire catchment. This enables the calibration of the (semi)distributed modelling framework in this study to use only a single parameter. The results without calibration suggest that, in the absence of discharge observations, reasonable estimates of catchment-scale runoff responses are possibly based on observations at the sub-REW (i.e. plot) scale. Thus, our study provides a platform for the
20 future development of low-dimensional and robust semi-distributed, physically-based discharge models in ungauged catchments.

1 Introduction

Among the vigorous attempts to improve the current generation of physically-based hydrological models for application at the meso and large scale, Reggiani et al. (1998,
25 1999) proposed a semi-distributed physically-based modelling framework called the Representative Elementary Watershed (REW) approach. In this approach, a set of

Full Screen / Esc

Printer-friendly Version

Interactive Discussion

coupled mass balance equations is formulated at the scale of a representative control volume, i.e. a watershed, by integrating the balance equations derived for hydrological zones that constitute REWs. Examples of such zones are the concentrated overland flow zone, saturated overland flow zone, and groundwater zone (Lee et al., 2007). REW

5 provides a novel modelling platform that incorporates the advantages of distributed and lumped conceptual modelling approaches. The REW approach is used as a blueprint for many catchment models, including REWv4.0 (Reggiani and Rientjes, 2005), RE-WASH (Zhang and Savenije, 2005), CREW (Lee et al., 2007), and THREW (Tian et al., 2006), which have been successfully applied in a number of natural catchments (e.g.

10 Fenicia et al., 2005; Varado et al., 2006; Mou et al., 2008). Apart from the purpose of making predictions in ungauged basins, the REW approach has also been used to provide more insight into the hydrological functioning of a catchment (e.g. Li et al., 2012; Tian et al., 2012) and to investigate nutrient dynamics in the natural environment (e.g. Li et al., 2010; Ye et al., 2012).

15 The crucial step in the implementation of the REW approach is to "close" a set of mass balance equations at REW scale (Zehe et al., 2006). This task involves the quantification of the hydrological mass exchange fluxes between hydrological zones within the REW using functional relationships of state variables, fluxes and REW properties, called the closure relations (Beven, 2006; Zehe and Sivapalan, 2007; Lee et al.,

20 2005). Identification of appropriate closure relations is a key to success of the REW approach (Reggiani and Rientjes, 2005; Zhang and Savenije, 2005). Previous work has focused on deriving, improving and refining existing closure relations (e.g. Reggiani and Rientjes, 2010; Zehe et al., 2006; Lee et al., 2007) including the use of a better parameterization scheme (e.g. Zhang et al., 2005). However, the process descriptions

25 used in the closure relations rely on small-scale laboratory-type physics formulated for homogeneous domains, whilst closure relations aim to simulate integrated hydrological fluxes at a larger scale of hillslope and sub-catchments (i.e. REW scale). Thus, the immense challenge remains to achieve closure schemes that can rigorously cope with

well-known problems in scientific hydrology, such as scale-dependent effects, process non-linearity, sub-REW heterogeneities, and hysteresis (Beven, 2006).

Following theoretical frameworks discussed by Beven (2006), Vannametee et al. (2012) developed closure relations for concentrated overland flow (i.e. Hortonian runoff) in which the scaling effects on runoff generation were considered and explicitly treated in the structure of closure relations. Development of the closure relations was done following the aggregation-disaggregation approach as proposed by Robinson and Sivapalan (1995) and Viney and Sivapalan (2004). Closure relations were identified and parameterized using the Hortonian runoff flux generated with processes operating at the local scale. This was done by using a physically-based high-resolution model that generates a synthetic discharge data set for an extensive set of REWs and rainstorm characteristics (approximately 65 000 scenarios). Calibration of the closure relations against this data set resulted in a set of REW-scale parameters that compensates for scale transfer effects. These parameters, called scaling parameters, characterize the effects of REW geometry and sub-REW process variability in the generation of REW-scale Hortonian runoff. The scaling parameters were then related to rainstorm characteristics and locally observable REW properties such as REW geometry and infiltration capacity. Based on this relation, the scaling parameters can directly be estimated from observable REW characteristics and measureable boundary conditions without the need for calibration of conceptual parameters. Vannametee et al. (2012) showed that Hortonian runoff generated from the closure relations is in good agreement with that from the original physically-based high-resolution model.

Here we evaluate the proposed approach using real-world data at the catchment scale. The primary objective is to test and assess the applicability of the closure relations developed by Vannametee et al. (2012) in real catchments under different rainstorm conditions. Also, we investigate the improvement in the model's predictive capability as a result of the use of scaling parameters by a comparison of model results with a standard rainfall-runoff model that does not incorporate scaling parameters. The performance of the model with closure relations was evaluated against observed

discharge. We specifically address the following research questions: (1) How suitable are the closure relations as proposed in Vannametee et al. (2012) for simulating observed catchment-scale hydrologic responses (i.e. hydrograph and total discharge volume)? (2) What are the advantages of using the closure relations representing sub-REW processes over using a simple lumped rainfall-runoff model that neglects these processes?

The closure relations were applied to a small test catchment in the French Alps. The catchment was disaggregated into a number of REWs, each representing an individual geomorphologic unit. The closure relations, including the scaling parameters, were parameterized for individual REWs using measurable properties (e.g. hillslope geometry, saturated hydraulic conductivity, and so on) and rainstorm characteristics observed in the field. Discharge was simulated for individual REWs and subsequently routed over the drainage network. Evaluation of the closure relation's performance was done using the observed discharge at the catchment outlets for calibrated and non-calibrated closure relations. The same procedure was repeated by using a model without scaling parameters (i.e. without within-REW scaling), to serve as a benchmark.

This paper is organized in three main parts. The first part describes the methodology and the application of closure relations in the test catchment (i.e. description of the closure relations, derivation of REWs, parameterization of the closure relations, and calibration of closure relations against field data). In the second part we present the evaluation results and performance for both types of closure relations (i.e. with and without scaling parameters). In the last section we analyse and discuss the predictive performance, and assess the improvements gained from using the closure relations with scaling parameters.

Title Page

Abstract | Introduction

Conclusions | References

Tables | Figures

◄◄ | ►►

◄ | ►

Back | Close

Full Screen / Esc

2 Methodology

2.1 Catchment-scale rainfall-runoff modelling framework with REW approach

The catchment is disaggregated into a number of REWs. The model consists of two components: Hortonian runoff generation within the REWs and routing of these runoff responses at the catchment scale (Fig. 1). At the REW scale, runoff generation is simulated using two approaches. One approach uses the closure relation proposed by Vannametee et al. (2012). As a benchmark we use another closure relation that does not include scaling parameters. The simulation is done over time t, using a time step (Δt) of 5 min for all components. Below, the symbols used in the equations represent properties at an individual REW, except if indicated otherwise. If properties of multiple REWs are presented in the same equation, the subscript i is used to indicate properties of each individual REW$_i$.

2.1.1 REW closure relations

Closure relations using the scaling parameters

A brief summary of the closure relation using the scaling parameters developed by Vannametee et al. (2012), denoted as C, is presented here. For each REW, the change in the surface water storage S_t (m) of the Hortonian runoff zone (Lee et al., 2005) is modelled as:

$$\frac{dS_t}{dt} = e_{\text{ctop},t} - e_{\text{cu},t} - e_{\text{co,cr},t} \tag{1}$$

In Eq. (1), t is time (h); $e_{\text{ctop},t}$ (m h^{-1}) is the net rain flux at t; $e_{\text{cu},t}$ (m h^{-1}) is the infiltration flux to the unsaturated zone at t; and $e_{\text{co,cr},t}$ (m h^{-1}) is the outgoing runoff flux of the domain to the saturated overland flow and channel zones.

The proportion of the REW where Hortonian runoff occurs changes over time. The REW-scale infiltration flux is determined as a function of both water availability at the soil surface and the maximum infiltration capacity (i.e. potential infiltration rate) of the Hortonian runoff zone, and takes account of the runon-runoff process within the REWs during a rain event. Using the Green and Ampt infiltration equation (Saghafian et al., 1995), the closure relation for the REW-scale infiltration flux is defined as:

$$e_{\text{cu},t} = \min\left[\left(e_{\text{ctop},t} \cdot \Delta t\right) + S_t, \rho_t \cdot K_s \left(1 + \frac{H_f(\eta - \theta)}{F_t}\right) \cdot \Delta t\right] \Big/ \Delta t \qquad (2)$$

In Eq. (2), "min $[x, y]$" selects the lesser value of x (i.e. the depth of water available for infiltration) and y (i.e. potential infiltration depth at t over the Hortonian runoff zone); ρ_t (–) is the ponding fraction at t, representing the proportion of the REW with Hortonian runoff and infiltration; K_s (m h^{-1}) is the saturated hydraulic conductivity; H_f (m) is the matric suction at the wetting front; η (–) is the soil effective porosity; θ (–) is the antecedent moisture content; and F_t (m) is the cumulative infiltration at t. During the rainstorm infiltrating water is supplied by rainwater and the infiltration flux is spatially uniform over the REWs; the ponding fraction is assumed to be one. After the storm period, the infiltration flux becomes spatially variable and the extent of the Hortonian runoff zone (i.e. ponded area) decreases over time. This is related to the flow pattern that determines the spatial pattern of runoff in the REWs (Vannametee et al., 2012). The ponding fraction is modelled as:

$$\rho_t = a \cdot S_{t-\Delta t} \; ; \; t \notin T$$
$$= 1 \qquad ; t \in T \qquad (3)$$

with, a (m^{-1}), the ponding factor, a scaling parameter related to the spatial variation in runoff and infiltration; T, a set of the time domain during which the REWs receives rainwater. Note that rainstorms are modelled as distinct events in time.

Discharge from the REW is simulated using a linear reservoir and related to surface storage. As hydrologic responses are not instantaneous, we use a past state of the

REW storage to calculate the responses at the time of interest, accounting for travel times over the slope. The Hortonian runoff flux leaving the REW to the channel is, thus, modelled as:

$$e_{\text{co,cr},t} = b \cdot S_{t-c}; t > c$$
$$= 0; t \leq c \tag{4}$$

And, discharge from the REW (Q_t; m³ h⁻¹) is calculated as:

$$Q_t = e_{\text{co,cr},t} \cdot A \tag{5}$$

In Eq. (4), b (h⁻¹) is the reservoir parameter, a scaling parameter representing the storage properties of the REW; c (h) is the third scaling parameter, a lag time representing the delay in REW storage in releasing water; S_{t-c} (m) is the storage in the REW, expressed as a depth of water layer at the surface at $t - c$; A (m²) is the area of the REW.

The three scaling parameters (i.e. a, b, and c) can be directly estimated for each REW from eight observable parameters. These are the rainstorm characteristics, average storm intensity R_{avg} (m h⁻¹), storm duration T (h), and a number of characteristics of the REW itself: slope gradient s (–), slope length L (m), micro relief c_1 (m), saturated hydraulic conductivity, matric suction at the wetting front, and initial moisture content. Following Vannametee et al. (2012), estimation of the value of these parameters is done by distance-weighted interpolation between points in a large database (approximately 65 000 scenarios) of these observable characteristics with associated scaling parameters.

Closure relations without scaling parameters

In order to evaluate the performance of the closure relation C, we use another closure relation which has a similar form to the closure relations described above but without the scaling components, referred to as C^*. This is done by using fixed values of the

Title Page

Abstract | Introduction

Conclusions | References

Tables | Figures

|◄ | ►|

◄ | ►

Back | Close

Full Screen / Esc

Printer-friendly Version

Interactive Discussion

scaling parameters; $a = 1$ in Eq. (3) and $b = 1$, $c = 0$ in Eq. (4). The latter implies an instantaneous runoff response from the REWs. The outgoing runoff flux at t is simply a surplus of the net rain flux at t after abstracting the infiltration flux at t:

$$e^*_{co,cr,t} = e_{ctop,t} + e^*_{cu,t} \tag{6}$$

5 The superscript $*$ indicates that the fluxes are calculated from the closure relation C^*. In Eq. (6), multiplication of $e^*_{co,cr,t}$ by the area of the REWs results in the discharge of the REWs (i.e. Eq. 5). Note that infiltration after the rain events is neglected. Without storage capacity, the past state of the REW storage, $S_{t-\Delta t}$, in Eq. (3) is zero, which also results in a ponding fraction, ρ_t, of zero for the REWs. The infiltration flux in Eq. (3)
10 can be rewritten as:

$$
\begin{aligned}
e^*_{cu,t} &= \min\left[e_{ctop,t}, K_s\left(1 + \frac{H_f(\eta - \theta)}{F_t}\right)\right] ; t \in T \\
&= 0 ; t \notin T
\end{aligned}
\tag{7}
$$

2.1.2 Runoff generation at the catchment level

Discharge Q_t generated from each REW is assumed to flow directly to the channel
15 network, which drains water to the outflow point of the catchment. We assume no gain or loss of water in the channel zone by other processes (i.e. channel precipitation, infiltration, and evaporation) as these are considered to have a minor influence on the amount of discharge volume at the catchment scale. The travel time C_i (h) of discharge from REW$_i$ to the catchment outlet is calculated as:

20 $$C_i = \frac{D_i}{\left(\left(A_r/P\right)^{2/3} \cdot \sqrt{S_i} \cdot n^{-1} \right)} \tag{8}$$

In Eq. (8), D_i (m) is the distance over the drainage network from the outlet of REW$_i$ to the catchment outlet. The denominator is the flow velocity (m h^{-1}) along the channel,

calculated using Manning's formula, with A_r (m^2) the average channel cross-section, P (m) the wetted perimeter, S_i (–) the averaged channel slope gradient along the flow path from the outlet of REW$_i$ to the catchment outlet, n (h m$^{-1/3}$) the manning's roughness coefficient of the channel.

5   The discharge at the catchment scale at t ($Q_{W,t}$; m^3 h^{-1}) can be derived as a sum of the discharges generated from all individual REWs that reach the outlet at t:

$$Q_{W,t} = \sum_{i=1}^{N} Q_{i,t-C_i} \tag{9}$$

where $Q_{i,t-C_i}$ is the discharge (m^3 h^{-1}) generated from REW$_i$ at $t - C_i$; N is the total number of REWs.

10 **2.1.3 Forcing and boundary conditions of the REWs**

Model forcing and boundary conditions required for the closure relations are net rain flux and antecedent moisture content before the events start, derived for individual REWs. Since these components are not part of the closure relation for Hortonian runoff, description of these components is given in a separate section.

15   Net rain flux is defined as the rain flux that reaches the soil surface of the REW after subtraction of the interception:

$$e_{\text{ctop},t} = R_t - \min\left[(R_t \cdot v_{\text{cov}}), \left(\frac{S_{l,\max} - S_{l,t-1}}{\Delta t}\right)\right] \tag{10}$$

$$v_{\text{cov}} = e^{-k \cdot \text{LAI}} \tag{11}$$

20

$$S_{l,\max} = \text{LAI} \cdot S_{l,\text{leaf}} \tag{12}$$

1778

$$S_{l,t} = \min(S_{l,\max}, S_{l,t-1} + e_{\text{ctop},t-1}) \tag{13}$$

In Eq. (10), R_t (m h^{-1}) is the rain flux. The second term represents the interception, in which v_{cov} (–) is the vegetation cover, estimated by the Beer-Lambert equation (Bulcock and Jewitt, 2010), $S_{l,\max}$ (m) is the maximum content of the interception storage, and $S_{l,t}$ (m) is the actual interception storage. In Eq. (11) and (12), k (–) is a light extinction coefficient, LAI (–) is the leaf area index, $S_{l,\text{leaf}}$ (m) is the maximum storage capacity per unit leaf area. We assume no canopy loss during events. Furthermore, it is assumed that the rainwater intercepted by the canopy does not reach the soil surface and has completely evaporated after the event. The canopy interception storage is, thus, empty at the start of the following event.

As initial soil moisture content at the start of the events was not monitored in the field, a simple soil water balance model of the unsaturated zone is used to obtain the initial soil water content for an individual REW at the start of the events. We assume large enough groundwater depth such that there is no influence of groundwater on the upper soil zone. Soil moisture content of individual REWs at t (θ_t) is estimated by:

$$\theta_t = \max\left[\min\left[\left(\frac{S_{\text{rz},t} + R_t \cdot \Delta t - E_{a,t}}{r}\right), \theta_s\right], \theta_{\text{PWP}}\right] \tag{14}$$

where $S_{\text{rz},t}$ (m) is the soil water in the root zone, r (m) the averaged root-zone depth of the catchment, $E_{a,t}$ (m) the actual evapotranspiration flux, θ_s (–) the soil moisture content at saturation, and θ_{PWP} (–) the soil moisture content at permanent wilting point. Note here that r, θ_s, and θ_{PWP} are assumed constant for all REWs, and that θ_s equals soil porosity. The actual evapotranspiration can be estimated as a function of the potential evapotranspiration $E_{p,t}$ (m), soil water availability, and soil water stress (Xia and Shao, 2008):

$$E_{a,t} = E_{p,t}; \quad k_{\theta,t} \geq k_\theta^*$$

$$\quad = E_{p,t} \cdot k_{\theta,t} \cdot \frac{1}{k_\theta^*}; \quad k_{\theta,t} < k_\theta^* \tag{15}$$

$$k_{\theta,t} = \frac{\theta_t - \theta_{PWP}}{\theta_{fc} - \theta_{PWP}} \tag{16}$$

where $k_{\theta,t}$ (−) is the fraction of readily available water for plants in the root zone of the REW. k_θ^* (−) is the critical threshold below which the soil is considered under water stress, commonly set at 0.5 or at a moisture content of half the soil moisture content at field capacity, θ_{fc} (−) (Dingman, 2002; Gervais et al., 2012). At this point, soil water availability for plants is limited and the actual evapotranspiration rate becomes less than the potential evapotranspiration (Pereira et al., 1999).

The potential evapotranspiration flux is assumed as spatially uniform over the catchment. $E_{p,t}$ used in Eq. (14) was derived by evenly distributing the monthly potential evapotranspiration, estimated using the modified Thornthwaite method (Xu and Singh, 2001), for each time step of Δt. Monthly potential evapotranspiration is estimated as:

$$E_p = \frac{4}{3} \cdot \frac{N_m}{30} \cdot l_d \cdot \left(\frac{10 \cdot \overline{T_m}}{l_h} \right)^\lambda \tag{17}$$

$$l_h = \sum_{m=1}^{12} \left(\frac{\overline{T_m}}{5} \right)^{1.51} \tag{18}$$

$$\lambda = 6.7 \cdot 10^{-7} \cdot l_h^3 - 7.7 \cdot 10^{-5} \cdot l_h^2 + 1.8 \cdot 10^{-2} \cdot l_h + 0.49 \tag{19}$$

where N_m (days) is the number of days in a given month m; l_d (h) is the average monthly day length. l_h (°C) is an annual heat index; $\overline{T_m}$ (°C) is the mean monthly air temperature of a month m; λ is an empirical coefficient.

2.2 Catchment and observations

2.2.1 Description of the catchment

The catchment is a first-order sub-basin of the Buëch catchment, located near the village of Savournon in the French pre-Alps region. The catchment has a size of 15.7 km^2
with an elevation range of 710–1780 m (Fig. 2). The region has a Mediterranean climate
with Alpine influences (Van Steijn and Hétu, 1997). Lithology of the test catchment is
characterized by deposits of Callovian-Oxfordian black marls, known as "Terres Noires"
(Descroix and Gautier, 2002; Oostwoud Wijdenes and Ergenzinger, 1998; Giraud et
al., 2009), which are found below the "Calcaire Tithonique" limestone. The morphology
of the catchment is mainly shaped by periglacial processes during the Pleistocene.
The upper part of the catchment is dominated by steep scree slopes below "Calcaire
Tithonique" limestone hogbacks. Eroded materials from the upslope area contribute to
the formation of extensive fan-shape alluvial deposits at the flat part of the catchment,
on which the major land use activities are pasture and agriculture. Intensive erosion on
highly-erodible marly deposits on the steep areas results in the formation of a badlands
topography and deep-cut gullies (Mathys and Klotz, 2008). Vegetation characteristics
in the catchment are quite variable, ranging from Mediterranean shrubs to a number of
deciduous and alpine coniferous species.

2.2.2 Field data collection

Meteorology and discharge

A meteo station was installed approximately at the centre of the catchment. Temperature, air pressure, relative humidity, incoming solar radiation, wind speed and wind
direction were recorded as an average state for 0.5 h intervals. Rainfall data were collected at 12 locations over the period of March to October 2010 (Fig. 2) by using tipping
bucket rain gauges with a bucket volume representing 0.2 mm of rain.

Discharge data were collected at 3 locations (Fig. 2). Upstream areas (i.e. sub-catchments) above the gauging locations are 11.9, 3.8, and 0.6 km^2, referred to in this paper as a Large (L), Medium-sized (M) and Small (S) catchment, respectively (Fig. 3). L and M are independent and assumed to have no hydrological influence on each other, whereas S is nested in M (i.e. a sub-catchment of M). The water stage at these locations was continuously recorded using pressure transducers. Stream discharge was measured 15–20 times at each location using salt dilution gauging with the slug injection method (Hendriks, 2010; Moore, 2004). Relations between discharge and corresponding water stage were constructed, resulting in a stage-discharge rating curve at each measurement location, from which the discharge time series of 3 catchments were obtained accordingly.

Estimation of the volume of Hortonian runoff was done on an event basis using a graphical method (Hendriks, 2010). A straight line was projected from the start of the hydrograph rising to intersect the hydrograph at the falling limb, where the contribution of the Hortonian runoff to the event's discharge had ended. The partition of discharge above this straight line is considered as Hortonian runoff. The runoff partition point was indicated where the slope of the hydrograph or slope of the recession coefficient in the recession limb is inflected in the semi-logarithm plot (Blume et al., 2007). If several inflection points were observed on the recession limb, the point that falls during the period at which the Hortonain runoff was expected to cease was chosen. In practice, such a point usually appeared as first or earliest on the recession limb because the Hortonian runoff mechanism is a fast process.

Geomorphology, vegetation and delineation of the REWs

Topography, morphology of the landscape, geologic parent material, and characteristics of the sediment deposits at the surface and near-surface were investigated throughout the catchment. Soil texture and regolith thickness were also estimated at a number of locations. The orientation of the hill slope relative to the channel network and catchment drainage system was also noted. These observations were used to map the

landscape's geomorphic characteristics and resulted in the geomorphological map of the catchment (i.e. see Sect. 3.1).

Vegetation was observed and mapped as units of relatively uniform vegetation types (Fig. 3). For each vegetation unit, a number of plots with a size of $100\,m^2$ (i.e. 10–15 plots) was randomly chosen. The proportion of the area covered by vegetation in each plot was visually estimated and averaged to obtain a representative vegetation cover for each vegetation unit.

Information on geomorphology, vegetation and the drainage network are crucial in the disaggregation of the study catchment into a number of REWs. The REWs were delineated using the concept of hydrologic landscape units (Winter, 2001) such that the REWs can be thought of as uniform in terms of genesis, structural pattern and hydrological properties. In this study, REWs were derived by subdividing the major geomorphologic units into more fundamental landscape units with distinct vegetation and regolith properties. The boundaries of the units were defined by the local watershed divide or coincided with the channels to which the units drain. This delineation rule simplifies our case study by restricting the REW's incoming flux only to the net rain. REWs do not receive the cross-boundary surface runoff flux from adjacent REWs (i.e. runon). Hydrologic properties and processes operating over individual REWs can be regarded as relatively homogeneous.

2.3 Parameterization in the modelling framework

Forcing data, boundary conditions, and properties of individual REWs were obtained from field observation or taken from various sources of reference. Details of the parameterization methods and parameter values used in the closure relations are presented in Table 1.

2.4 Calibration and evaluation of closure relations

For the scenarios with calibration of closure relations, calibration was performed by matching the observed discharge at each catchment outlet. We used a simple split-sample approach for the calibration. Two sets of events, in total approximately half of all events observed in each catchment, were randomly selected for calibration and validation. As we focus on the capacity of the closure relations to produce accurate discharge responses (i.e. the shape of hydrograph), the objective function used in the calibration is the Nash-Sutcliffe efficiency index, E (–):

$$E = 1 - \frac{\sum_{t=1}^{T_{end}} (Q_{t,m} - Q_{t,\text{obs}})^2}{\sum_{t=1}^{T_{end}} (Q_{t,\text{obs}} - \bar{Q}_{\text{obs}})^2} \tag{20}$$

where T_{end} is the end time of simulation; $Q_{t,m}$ ($\text{m}^3 \text{h}^{-1}$) is discharge simulated at t from the closure relations, $Q_{t,\text{obs}}$ ($\text{m}^3 \text{h}^{-1}$) is the observed discharge at t; and $\bar{Q}_{\text{obs}}$ ($\text{m}^3 \text{h}^{-1}$) is the mean observed discharge. This calibration procedure was used for the model using both closure relations C and C^*.

The saturated hydraulic conductivity K_s was chosen for calibration because it is a key parameter governing the mechanism of Hortonian runoff generation, and because the closure relations are most sensitive to this parameter (Vannametee et al., 2012). Calibration of K_s was done by adjusting a single prefactor, added to K_s as a multiplier (i.e. calibration factor) for the entire domain, using a brute force calibration approach. The calibration factors were defined as a sequence of discrete values ranging from 0.1 to 500. The optimal calibration factor of K_s is the value that results in the best E, evaluated for all calibration events. To avoid the effect of outliers, we used the median.

It is preferable to use a single optimal calibration factor that is suited for all events observed in all catchments. This is to satisfy the assumption used in the parameterization

of K_s to the REWs that soil hydraulic properties of specific geomorphologic units are invariant in the catchment, and also to maintain the relative order of K_s values for the REWs after calibration. However, physical characteristics of the S catchment are significantly different from the other catchments. More than 90 % of the S catchment area is dominated by a badlands topography and scree slopes with sparse vegetation cover, while the other two catchments are mainly characterized by alluvium or colluvium deposits with agricultural activities and forests. Including events from the S catchment would introduce a bias in the identification of the optimal calibration factor for the entire catchment. Therefore, a second optimal calibration factor was exclusively derived for the S catchment. The optimal calibration factor for L and M catchments were identified together because the physiographic characteristics are quite comparable between these catchments.

We evaluated the performance of the models using the closure relation C and C^* (both with and without calibration) with a separate set of events not used in the calibration (i.e. validation set). Performance of the closure relations was evaluated in terms of response signature (i.e. hydrograph), measured with E, and discharge quantity. Percent error in discharge volume ($e_{Q_{cum}}$) is computed as:

$$e_{Q_{cum}} = \left| \frac{Q_{cum,sim} - Q_{cum,obs}}{Q_{cum,obs}} \right| \cdot 100 \tag{21}$$

with $Q_{cum,obs}$ and $Q_{cum,sim}$ (m^3) being the total observed and simulated discharge volume, respectively.

3   Results

3.1   Identification of REWs and catchment discharge

The catchment was classified into 11 types of major geomorphologic units, from which 59 REWs were derived (Fig. 4, Table 3). More than 30 rainstorm events were observed

during the study period (Table 4). For the evaluation of the closure relations we neglected the events with an insignificant contribution of Hortonian runoff to the total event discharge, i.e. those events with a Hortonian runoff coefficient below 1.5 %. In total, 10 events were not used in the evaluation of the closure relation performance. For these events it is likely that the stream discharge was dominated by processes not accounted for in the closure relations, for instance direct channel precipitation (i.e. stream channels possess about 1.5 % of the catchment area). We selected events where Hortonian runoff (i.e. quick flow) can be clearly identified and partitioned from the base flow component. These events are mainly observed in summer and autumn (i.e., July–October), occurring as isolated events with a relatively high intensity (i.e. $R_{t,\mathrm{avg}}$ up to $0.03\,\mathrm{m\,h^{-1}}$ with a maximum of $0.1\,\mathrm{m\,h^{-1}}$ in 5 min). It is relatively easy to derive the event duration and Hortonian runoff for these events. However, this was not the case for events observed in spring and early summer for which hydrograph separation was difficult. These events consisted of a set of consecutive light rainstorms which resulted in complex hydrographs with multiple peaks that do not have a clear rising and falling limb.

3.2 Modelled discharge without calibration

Performance in terms of the Nash-Sutcliffe index (E) shows that the closure relation C is capable of simulating discharge responses better than the benchmark closure relation C^* (Fig. 5a, c and Table 5). With simulation using the closure relation C, more than 30 % of the events in the three catchments have an E value above zero (Fig. 5a). About 75 % of these events (i.e., E above zero) occurred in the S catchment. Furthermore, only 25 % of the total events observed in the S catchment have an E below zero. On the contrary, simulation of discharge responses using the closure relation C^* results in negative E values for most events in all catchments (Fig. 5c). This indicates that the closure relation C^* has almost no predictive capability and that the mean observed discharge would be a better predictor than the closure relation C^*.

Hydrographs of an individual event (Fig. 6a, c and e) simulated by the closure relation C^* exhibit an almost instantaneous discharge response to rainfall, resulting in hydrographs that closely follow rainfall intensity and severely overestimate runoff response. The closure relation C, on the other hand, produces a smoother hydrograph with more delay in runoff responses relative to the rainfall. Although the magnitude of discharge is overestimated when using the closure relation C, the shape of the modelled hydrograph is comparable to the observed hydrograph. The discrepancy between observed and modelled hydrographs is smallest for the S catchment.

Errors in total discharge volume are also larger for the simulation with closure relation C^* compared to C (Table 5), particularly for the catchment S. Regardless of the closure relation used, the discharge volume is generally overestimated by the models, apart from the S catchment where discharge volume is underestimated for events with a relatively high rainfall intensity.

3.3 Simulation of discharge with calibration

3.3.1 Derivation of the calibration factors

Characteristics of the calibration events (Table 6), except for event duration, are not statistically different to those of the events used for validation of the closure relations, according to statistical tests on mean and variance differences (not shown). Also, the predictive performance of closure relations for these two event groups is quite comparable (Table 7). It can be asserted that the events used for calibration have similar characteristics to the events for validation. Thus, the optimal calibration factors can be derived without a remarkable bias caused by differences between the calibration and validation events.

Figure 7a and b show the values of the Nash-Sutcliffe coefficient (E) for different calibration factors. Although we aim at deriving optimal calibration factors based on E, effects of the calibration factor on the percent error in discharge volume, $e_{Q_{\text{cum}}}$, were also investigated (Fig. 7c and d), providing insight into the capability of closure relations

1787

to predict the discharge volume. The optimal calibration factor for each catchment can be visually identified from the highest point in the response line of the Nash Sutcliffe coefficient; and the lowest point in the response line of $e_{Q_{cum}}$.

For the closure relation C, the response line for the Nash Sutcliffe coefficient clearly shows a single optimum. According to Fig. 7a, the optimal calibration factor of 12 found for the L and M catchment is larger than the value obtained for the S catchment, which was 5. For the S catchment, a calibration factor of 1 results in almost as good results as a factor of 5. This supports the findings in Sect. 3.2 that the closure relation C already performs reasonably well for this catchment without calibration (i.e. calibration factor = 1). The calibration factors resulting in the lowest median of E are not very different from those resulting in the lowest median of $e_{Q_{cum}}$ (Fig. 7a and c), allowing the single value that scores well on both E and $e_{Q_{cum}}$.

It is difficult to identify a single optimal calibration factor for the closure relation C^*. The median of E gradually increases with an increase in the calibration factor, but never exceeds zero (Fig. 7b). The best median of E was found at an extremely high calibration factor. Here, we selected the highest calibration factor, 200, as an optimum for the L and M catchment, while a calibration factor of 20 was chosen for the S catchment. Unlike the response line for the Nash Sutcliffe coefficient, the line for $e_{Q_{cum}}$ shows a clear optimum (Fig. 7d). Note that the optimal calibration factors for closure relation C^* for $e_{Q_{cum}}$ are similar to the values obtained for closure relation C (Fig. 7c and d). As we aim to optimize E, the calibration factor selected from E, as described above, is used for the validation.

3.3.2 Validation results

The performance of the calibrated closure relation C is considerably better than the non-calibrated case, as can be seen by a large improvement in discharge prediction in the right-panel plots compared to the left-panel plots in Fig. 5. Approximately 65 % of the validation events have an E value above zero (Fig. 5b). The best E obtained after calibration is 0.8 with a median of 0.3, which is slightly worse than what is found

1788

for the calibration events (i.e. 0.4). Unlike the closure relation C^*, the results show that C is capable of reproducing both the observed total discharge and hydrograph shape for most events (Fig. 5d) after calibration using a single calibration factor. This result could already be expected because the optimal calibration factors that result in the lowest median of $e_{Q_{\text{cum}}}$ are comparable to the factors resulting in the best median of E (Fig. 7a and c). Predictive capability of the closure relation C is somehow exacerbated after calibration for a number of events observed in the S catchment, as shown by a lower median of E compared to the case of using the non-calibrated closure relation C (Table 8).

The capability of the benchmark closure relation C^* in simulating the hydrograph shape is not satisfactorily improved by calibration. The median E calculated for the validation events is still below zero for all catchments (Table 8), and almost 80 % of events have an E between -1 and 0 (Fig. 5d). Although the magnitude of the modelled discharge is comparable to the observed discharge, the shape of the hydrograph is incorrect (Fig. 6b, d, and f). As shown in Fig. 8, the shape of the hydrograph barely changes with calibration factors, in that the response to rainfall remains too instantaneous. This results from the inability of the closure relation C^* to account for sub-REW runon-runoff processes, changes in ponded areas, and runoff travel times within individual REWs. However, a better estimate of the discharge volume can be achieved after calibration when using the different calibration factors (Fig. 8b, d and f). We can conclude here that it is only feasible to calibrate the closure relation C^* to have a correct discharge volume, but not for a correct shape of the hydrograph.

Investigation of the performance of the calibrated closure relations for various event characteristics shows that the closure relation C has predictive power (i.e. $E > 0$) for events with a runoff coefficient larger than 0.02 (Fig. 9a), while performance both in terms of E and $e_{Q_{\text{cum}}}$ is highest for events with a runoff coefficient between 0.05–0.1, and gradually decreases with increasing runoff coefficient. Relations between $e_{Q_{\text{cum}}}$ and the runoff coefficient (Fig. 9b) show a pattern comparable to those found for E, showing smallest discharge volume errors at intermediate values of the runoff

coefficient. The value of $e_{Q_{cum}}$ reaches almost 100 % at high values of the runoff coefficient (Fig. 9b). This indicates that, for the calibrated closure relation C, discharge is underestimated for the events with a high runoff coefficient. The optimal performance of closure relation C after calibration for events with a moderate runoff coefficient is due to the use of a calibration factor that results in the best median value of E for all events. For events with a very low runoff coefficient, the discharge volume is still largely overestimated, which is also the case for the simulation with the non-calibrated closure relation C.

Unlike the closure relation C, the closure relation C^* does not exhibit a trend in performance as a function of the runoff coefficient because the discharge responses were poorly simulated for most events.

4 Discussion and conclusion

This study aimed at evaluating, at the catchment scale, the performance of a previously-developed closure relation for REW-scale Hortonian runoff. This closure relation, C, incorporates scaling parameters to account for sub-REW process heterogeneity. The value of these scaling parameters can be calculated as a function of rainstorm characteristics and measurable REW properties, using relations derived from an extensive synthetic data set, given in Vannametee et al. (2012). The closure relation was incorporated in a rainfall-runoff model, which was applied to a first-order catchment in the French Alps. The catchment was divided into 60 REW units corresponding to dominant geomorphological features. Performance of the closure relation C was evaluated on an event basis against discharge observed at 3 locations in the catchment. To assess the relative performance of our closure relation, results were compared to results from a benchmark closure relation C^* that does not incorporate scaling parameters.

The results show that the closure relation C clearly outperforms the benchmark closure relation C^*, with respect to the Nash Sutcliffe coefficient and error in total discharge

volume for most events. The closure relation C is capable of reproducing the hydrograph shape for our study catchment, even without calibration. Shape and timing of responses of the simulated hydrographs by the non-calibrated C are in accordance with the observed discharge; however, the response magnitude and discharge vol-

5   umes are overestimated for a number of events. Contrary to our closure relation C, it is impossible to obtain accurate discharge responses using the closure relation C^* that does not correct for sub-REW processes. Discharge responses reproduced by C^* are too dependent on the temporal characteristics of storm intensities. Furthermore, the discharge volume is considerably overestimated.

10   Calibration of K_s in the closure relation C simultaneously improves the shape of the hydrograph and total discharge volume, resulting in K_s values that are 5–12 times higher than the original (uncalibrated) values. The calibrated K_s values are, however, still in the realistic range of values that are typically observed at the plot scale when using a rainfall simulation method (Robichaud, 2000; Harden and Scruggs, 2003; Stone

15   et al., 2008; Langhans et al., 2011; Van den Putte et al., 2012). Note that our calibrated K_s values represent local (plot) scale values, as the scale effects are isolated and explicitly accounted for by the scaling parameters in the closure relation C. Unlike the closure relation C, the benchmark closure relation C^* remains incapable of reproducing observed hydrographs after calibration. As the benchmark closure relation

20   C^* neglects scaling effects, process description is grossly simplified as analogous to the runoff-generation processes at a plot scale; runoff was modelled as an infiltration-excess flux that is instantaneously discharged from the REWs without delay, resulting in hydrographs with a too steep rising and falling limb compared to the observed hydrographs. Also, calibrated K_s values for the benchmark closure relation reach unrealistic

25   high values that do not have a physical meaning. Calibration of the benchmark closure relation C^* on discharge volume (instead of the Nash Sutcliffe index used in all calibration runs) gives reasonable results in terms of discharge volume, but the hydrographs remain far too peaked.

Title Page

Abstract | Introduction

Conclusions | References

Tables | Figures

|◄ | ►|

◄ | ►

Back | Close

Full Screen / Esc

Printer-friendly Version

Interactive Discussion

The increased capability of closure relation C in reproducing the discharge can be attributed to the use of scaling parameters, representing scaling effects and spatial processes within the REW. That is, the closure relation explicitly accounts for the effects of the REW's geometry (e.g., length, slope gradient, and connectivity in flow pattern) and sub-REW processes (e.g. post-event infiltration, REW storage) on the response characteristics at the REW scale (i.e. lag of responses, attenuation of responses, and so on). As a result, the closure relation C is capable of reproducing catchment-scale behaviour, even without calibration. Errors in the discharge magnitude of the non-calibrated runs can mainly be attributed to the uncertainty in the estimation of infiltration parameters (i.e. K_s and H_f) and boundary conditions in the closure relation C. It is shown that if the infiltration parameters were accurately estimated for the REWs, calibration is not needed. This can be seen in the discharge simulation of the S catchment, which consists of 3 REWs that have a small infiltration capacity. Infiltration parameters for these REWs can be estimated quite easily, which results in a good hydrograph prediction for a large number of events. For the benchmark closure relation C^*, calibration does not remarkably improve the discharge prediction, which is a strong indication that C^* does not properly capture the processes in the REWs. It might be possible to improve the performance of the benchmark closure relation C^* by calibrating a larger number of parameters. Even if this were possible, the performance of the benchmark closure relation would largely rely on calibration, without the benefit of using observable watershed characteristics as in our closure relation C. The result would be a model with a weaker physical basis compared to our closure relation, because the issue of model structural inadequacy (Gupta et al., 2012) is not resolved.

The closure relation C exhibits the largest predictive value for events with a relatively high runoff coefficient. Predictive capacity of the non-calibrated closure relation C decreases for events with a low runoff coefficient. For these events, the hydrograph magnitude and discharge volumes are grossly overestimated. This may have various causes. One is that the closure relation C does not take into account all aspects of the spatial heterogeneity of the REW properties and its effects on runoff generation. Spatial

variability of infiltration parameters becomes more important in the runoff generation for low-intensity events. A deterministic process conceptualization using uniform infiltration parameters is apparently not sufficient to capture the stochastic behaviour of infiltration and runoff generation processes (Corradini et al., 1998; Karssenberg, 2006). Another limitation of our closure relation is related to the limited information on the value of scaling parameters for low intensity rainstorms. This is because low intensity rainstorms were under-represented in the synthetic database used by Vannametee et al. (2012) to derive scaling parameters as a function of rainstorm characteristics. Finally, additional errors in hydrograph estimation may occur due to errors in model inputs or structural errors in modelling framework in which the closure relation is used. In this study, we neglected seasonal dynamics of the vegetation characteristics, which might affect interception and soil moisture. Also, overestimation of the event discharge can be partly attributed to the assumption that no water loss occurs in the streams. Even though the amount of in-stream loss is most likely relatively small compared to the discharge generated at the catchment scale, neglecting the in-stream loss is likely to result in an overestimation of the discharge for storm events with a small runoff coefficient. For these events, discharge is mostly generated from upstream REWs (i.e. hogback, debris slope, and badlands) due to a smaller infiltration capacity compared to the downstream REWs (i.e. colluvium and alluvial fan). Discharge generated at upstream REWs is likely to be lost to deeper groundwater from the channels before it reaches the outlets. The calibration of K_s partly and implicitly corrects for this error.

The good discharge simulation results in the real-world catchments reported in this study indicate that the framework proposed by Vannametee et al. (2012) should be adopted as an alternative blueprint in the identification of closure relations. This approach is particularly useful because it does not entirely depend on field observations that might be costly or difficult to obtain. The closure relations can be deduced using an artificial data set, generated by a distributed high-resolution model, as a surrogate of real-world data. Future research along the line of this paper could focus on the improvement of the relations between scaling parameters in the closure relations and

observable parameters for a wide range of conditions. This can be done by recalculating and extending the database to include more observable watershed characteristics in the estimation of scaling parameters and focus more on light rainstorms. Also, the level of physics used in the numerical model used to derive the relations between scaling parameters and observables could be further improved. More importantly, other runoff generating mechanisms at the catchment scale such as saturated overland flow, including groundwater flow and variably saturated areas could also be considered in the modelling framework to achieve a complete REW-based model. The closure relations for these hydrological components can be developed following the hillslope-storage Boussinesq approach (Troch, 2003). Due to the fast progress in computing technology, limitations related to the available computational resources and run time will no longer be an obstacle for the aforementioned tasks. Advantages and trade-offs in using the closure relation C (either the current or improved versions) in comparison to a distributed hydrological model should also be investigated for catchments with different sizes; this should be done in a systematic way by looking at the simulation run time, computational costs, model efficiency, and calibration efforts.

References

Ahrens, B.: Distance in spatial interpolation of daily rain gauge data, Hydrol. Earth Syst. Sci., 10, 197–208, doi:10.5194/hess-10-197-2006, 2006.

Beven, K.: Searching for the Holy Grail of scientific hydrology: $Q_t = (S, R, \Delta t)A$ as closure, Hydrol. Earth Syst. Sci., 10, 609–618, doi:10.5194/hess-10-609-2006, 2006.

Blume, T., Zehe, E., and Bronstert, A.: Rainfall – runoff response, event-based runoff coefficients and hydrograph separation, Hydrolog. Sci. J., 52, 843–862, doi:10.1623/hysj.52.5.843, 2007.

Breuer, L., Eckhardt, K., and Frede, H.-G.: Plant parameter values for models in temperate climates, Ecol. Model., 169, 237–293, doi:10.1016/S0304-3800(03)00274-6, 2003.

Brolsma, R. J., Karssenberg, D., and Bierkens, M. F. P.: Vegetation competition model for water and light limitation. I: Model description, one-dimensional competition and the influence of groundwater, Ecol. Model., 221, 1348–1363, doi:10.1016/j.ecolmodel.2010.02.012, 2010.

Bulcock, H. H. and Jewitt, G. P. W.: Spatial mapping of leaf area index using hyperspectral remote sensing for hydrological applications with a particular focus on canopy interception, Hydrol. Earth Syst. Sci., 14, 383–392, doi:10.5194/hess-14-383-2010, 2010.

Burrough, P. A. and McDonnell, R. A.: Principles of Geographical Information Systems, 5th Edn., Oxford University Press, New York., 2004.

Chow, V. T., Maidment, D. R., and Mays, L. W.: Applied Hydrology, McGraw Hill, New York, 1988.

Corradini, C., Morbidelli, R., and Melone, F.: On the interaction between infiltration and Hortonian runoff, J. Hydrol., 204, 52–67, doi:10.1016/S0022-1694(97)00100-5, 1998.

Descroix, L. and Gautier, E.: Water erosion in the southern French alps: climatic and human mechanisms, Catena, 50, 53–85, doi:10.1016/S0341-8162(02)00068-1, 2002.

Dingman, S. L.: Physical Hydrology, 2nd Edn., Prentice Hall, Upper Saddle River, New Jersey, 2002.

Fenicia, F., Zhang, G. P., Rientjes, T., Hoffmann, L., Pfister, L., and Savenije, H. H. G.: Numerical simulations of runoff generation with surface water-groundwater interactions in the Alzette river alluvial plain (Luxembourg), Phys. Chem. Earth, 30, 277–284, doi:10.1016/j.pce.2004.11.001, 2005.

Forsythe, W. C., Rykiel, E. J., Stahl, R. S., Wu, H., and Schoolfield, R. M.: A model comparison for daylength as a function of latitude and day of year, Ecol. Model., 80, 87–95, doi:10.1016/0304-3800(94)00034-F, 1995.

Gervais, M., Mkhabela, M., Bullock, P., Raddatz, R. and Finlay, G.: Comparison of standard and actual crop evapotranspiration estimates derived from different evapotranspiration methods on the Canadian Prairies, Hydrol. Process., 26, 1467–1477, doi:10.1002/hyp.8279, 2012.

Giraud, F., Courtinat, B., and Atrops, F.: Spatial distribution patterns of calcareous nannofossils across the Callovian-Oxfordian transition in the French Subalpine Basin, Mar. Micropaleontol., 72, 129–145, doi:10.1016/j.marmicro.2009.04.004, 2009.

Title Page

Abstract | Introduction

Conclusions | References

Tables | Figures

|◄ | ►|

◄ | ►

Back | Close

Full Screen / Esc

Printer-friendly Version

Interactive Discussion

Gupta, H. V., Clark, M. P., Vrugt, J. A., Abramowitz, G., and Ye, M.: Towards a compre-
hensive assessment of model structural adequacy, Water Resour. Res., 48, W08301,
doi:10.1029/2011WR011044, 2012.

Harden, C. P. and Scruggs, P. D.: Infiltration on mountain slopes: a comparison of three envi-
ronments, Geomorphology, 55, 5–24, doi:10.1016/S0169-555X(03)00129-6, 2003.

Hendriks, M. R.: Introduction to Physical Hydrology, Oxford University Press, New York, 2010.

Karssenberg, D.: Upscaling of saturated conductivity for Hortonian runoff modelling, Adv. Water
Resour., 29, 735–759, doi:10.1016/j.advwatres.2005.06.012, 2006.

Koivusalo, H., Kokkonen, T., Laurén, A., Ahtiainen, M., Karvonen, T., Mannerkoski, H., Pentti-
nen, S., Seuna, P., Starr, M., and Finér, L.: Parameterisation and application of a hillslope
hydrological model to assess impacts of a forest clear-cutting on runoff generation, Environ.
Modell. Softw., 21, 1324–1339, doi:10.1016/j.envsoft.2005.04.020, 2006.

Kuriakose, S. L., Van Beek, L. P. H., and Van Westen, C. J.: Parameterizing a physically
based shallow landslide model in a data poor region, Earth Surf. Proc. Land., 34, 867–881,
doi:10.1002/esp.1794, 2009.

Langhans, C., Govers, G., Diels, J., Leys, A., Clymans, W., Putte, A., and Van Den Valckx, J.:
Experimental rainfall-runoff data: Reconsidering the concept of infiltration capacity, J. Hydrol.,
399, 255–262, doi:10.1016/j.jhydrol.2011.01.005, 2011.

Lee, H., Sivapalan, M., and Zehe, E.: Representative Elementary Watershed (REW) approch, a
new blueprint for distributed hydrological modelling at the catchment scale, in Predictions in
Ungauged Basins: International Perspectives on the State of the Art and Pathways Forward,
edited by: Franks, S. W., Sivapalan, M., Takeuchi, K., and Tachikawa, Y., 159–188, IAHS
Publication, 301, Mepple, 2005.

Lee, H., Zehe, E., and Sivapalan, M.: Predictions of rainfall-runoff response and soil moisture
dynamics in a microscale catchment using the CREW model, Hydrol. Earth Syst. Sci., 11,
819–849, doi:10.5194/hess-11-819-2007, 2007.

Li, H., Sivapalan, M., Tian, F., and Liu, D.: Water and nutrient balances in a large tile-drained
agricultural catchment: a distributed modeling study, Hydrol. Earth Syst. Sci., 14, 2259–2275,
doi:10.5194/hess-14-2259-2010, 2010.

Li, H., Sivapalan, M., and Tian, F.: Comparative diagnostic analysis of runoff generation pro-
cesses in Oklahoma DMIP2 basins: The Blue River and the Illinois River, J. Hydrol., 418–419,
90–109, doi:10.1016/j.jhydrol.2010.08.005, 2012.

Mathys, N. and Klotz, S.: Draix: A field laboratory for research on hydrology and erosion in mountain areas, in Proceedings of the 4th Canadian Conference on Geohazards: From Causes to Management, edited by: Locat, D. J., Perret, D., and Turmel, D., 594 pp., Presse de l'Université Laval, Québec, 2008.

5 Moore, R. D.: Introduction to salt dilution gauging for streamflow measurement: Part 1, Streamline Watershed Management Bulletin, 7, 20–23, 2004.

Mou, L., Tian, F., Hu, H., and Sivapalan, M.: Extension of the Representative Elementary Watershed approach for cold regions: constitutive relationships and an application, Hydrol. Earth Syst. Sci., 12, 565–585, doi:10.5194/hess-12-565-2008, 2008.

10 Oostwoud Wijdenes, D. J. and Ergenzinger, P.: Erosion and sediment transport on steep marly hillslopes, Draix, Haute-Provence, France: an experimental field study, Catena, 33, 179–200, doi:10.1016/S0341-8162(98)00076-9, 1998.

Pereira, L. S., Perrier, A., Allen, R. G., and Alves, I.: Evapotranspiration: Concepts and Future Trends, J. Irrig. Drain. Eng.-ASCE, 125, 45–51, doi:10.1061/(ASCE)0733-15 9437(1999)125:2(45), 1999.

Rawls, W. J., Brakensiek, D. L., and Saxton, K. E.: Estimation of Soil Water Properties, T. ASAE, 25, 1316–1320, 1982.

Reggiani, P. and Rientjes, T. H. M.: Flux parameterization in the representative elementary watershed approach: Application to a natural basin, Water Resour. Res., 41, 1–18, 20 doi:10.1029/2004WR003693, 2005.

Reggiani, P. and Rientjes, T. H. M.: Closing horizontal groundwater fluxes with pipe network analysis: An application of the REW approach to an aquifer, Environ. Modell. Softw., 25, 1702–1712, doi:10.1016/j.envsoft.2010.04.019, 2010.

Reggiani, P., Sivapalan, M., and Majid Hassanizadeh, S.: A unifying framework for water-25 shed thermodynamics: balance equations for mass, momentum, energy and entropy, and the second law of thermodynamics, Adv. Water Resour., 22, 367–398, doi:10.1016/S0309-1708(98)00012-8, 1998.

Reggiani, P., Hassanizadeh, S. M., Sivapalan, M., and Gray, W. G.: A unifying framework for watershed thermodynamics: constitutive relationships, Adv. Water Resour., 23, 15–39, 30 doi:10.1016/S0309-1708(99)00005-6, 1999.

Robichaud, P. R.: Fire effects on infiltration rates after prescribed fire in Northern Rocky Mountain forests, USA, J. Hydrol., 231–232, 220–229, doi:10.1016/S0022-1694(00)00196-7, 2000.

Title Page

Abstract	Introduction
Conclusions	References
Tables	Figures

| ◄◄ | ►► |
| ◄ | ► |

| Back | Close |

Full Screen / Esc

Printer-friendly Version

Interactive Discussion

Robinson, J. S. and Sivapalan, M.: Catchment-scale runoff generation model by aggregation and similarity analyses, Hydrol. Process., 9, 555–574, doi:10.1002/hyp.3360090507, 1995.

Saghafian, B., Julien, P. Y., and Ogden, F. L.: Similarity in Catchment Response: 1. Stationary Rainstorms, Water Resour. Res., 31, 1533, doi:10.1029/95WR00518, 1995.

5 Scurlock, J. M. O., Asner, G. P., and Gower, S. T.: Worldwide Historical Estimates and Bibliography of Leaf Area Index, 1932–2000, Oak Ridge, Tennessee, 2001.

Van den Putte, A., Govers, G., Leys, A., Langhans, C., Clymans, W., and Diels, J.: Estimating the parameters of the Green-Ampt infiltration equation from rainfall simulation data: Why simpler is better, J. Hydrol., 476, 332–344, doi:10.1016/j.jhydrol.2012.10.051, 2012.

10 Van Steijn, H. and Hétu, B.: Rain-generated overland flow as a factor in the development of some stratified slope deposits: A case study from the Pays du Buëch (Préalpes, France), Geogr. Phys. Quatern., 51, 3–15, doi:10.7202/004884ar, 1997.

Stone, J. J., Paige, G. B., and Hawkins, R. H.: Rainfall intensiy-dependent infiltration rates on rangeland rainfall simulation plots, T. ASABE, 51, 45–53, 2008.

15 Tian, F., Hu, H., Lei, Z., and Sivapalan, M.: Extension of the Representative Elementary Watershed approach for cold regions via explicit treatment of energy related processes, Hydrol. Earth Syst. Sci., 10, 619–644, doi:10.5194/hess-10-619-2006, 2006.

Tian, F., Li, H., and Sivapalan, M.: Model diagnostic analysis of seasonal switching of runoff generation mechanisms in the Blue River basin, Oklahoma, J. Hydrol., 418–419, 136–149, doi:10.1016/j.jhydrol.2010.03.011, 2012.

Troch, P. A.: Hillslope-storage Boussinesq model for subsurface flow and variable source areas along complex hillslopes: 1. Formulation and characteristic response, Water Resour. Res., 39, 1316, doi:10.1029/2002WR001728, 2003.

Vannametee, E., Karssenberg, D., and Bierkens, M. F. P.: Towards closure relations in the Representative Elementary Watershed (REW) framework containing observable parameters: Relations for Hortonian overland flow, Adv. Water Resour., 43, 52–66, doi:10.1016/j.advwatres.2012.03.029, 2012.

Varado, N., Braud, I., Galle, S., Le Lay, M., Séguis, L., Kamagate, B., and Depraetere, C.: Multi-criteria assessment of the Representative Elementary Watershed approach on the Donga catchment (Benin) using a downward approach of model complexity, Hydrol. Earth Syst. Sci., 10, 427–442, doi:10.5194/hess-10-427-2006, 2006.

Title Page

Abstract | Introduction

Conclusions | References

Tables | Figures

◄◄ | ►►

◄ | ►

Back | Close

Full Screen / Esc

Printer-friendly Version

Interactive Discussion

Viney, N. R. and Sivapalan, M.: A framework for scaling of hydrologic conceptualizations based on a disaggregation-aggregation approach, Hydrol. Process., 18, 1395–1408, doi:10.1002/hyp.1419, 2004.

Winter, T. C.: The concept of hydrologic landscapes, J. Am. Water Resour. As., 37, 335–349, doi:10.1111/j.1752-1688.2001.tb00973.x, 2001.

Xia, Y. Q. and Shao, M. A.: Soil water carrying capacity for vegetation: A hydrologic and biogeochemical process model solution, Ecol. Model., 214, 112–124, doi:10.1016/j.ecolmodel.2008.01.024, 2008.

Xu, C.-Y. and Singh, V. P.: Evaluation and generalization of temperature-based methods for calculating evaporation, Hydrol. Process., 15, 305–319, doi:10.1002/hyp.119, 2001.

Ye, S., Covino, T. P., Sivapalan, M., Basu, N. B., Li, H.-Y., and Wang, S.-W.: Dissolved nutrient retention dynamics in river networks: A modeling investigation of transient flows and scale effects, Water Resour. Res., 48, W00J17, doi:10.1029/2011WR010508, 2012.

Zehe, E. and Sivapalan, M.: *Editorial* Towards a new generation of hydrological process models for the meso-scale: an introduction, Hydrol. Earth Syst. Sci., without page numbers, 2007.

Zehe, E., Lee, H., and Sivapalan, M.: Dynamical process upscaling for deriving catchment scale state variables and constitutive relations for meso-scale process models, Hydrol. Earth Syst. Sci., 10, 981–996, doi:10.5194/hess-10-981-2006, 2006.

Zhang, G. P. and Savenije, H. H. G.: Rainfall-runoff modelling in a catchment with a complex groundwater flow system: application of the Representative Elementary Watershed (REW) approach, Hydrol. Earth Syst. Sci., 9, 243–261, doi:10.5194/hess-9-243-2005, 2005.

Zhang, G. P., Fenicia, F., Rientjes, T. H. M., Reggiani, P., and Savenije, H. H. G.: Modeling runoff generation in the Geer river basin with improved model parameterizations to the REW approach, Phys. Chem. Earth, 30, 285–296, doi:10.1016/j.pce.2004.11.002, 2005.

Title Page

Abstract | Introduction

Conclusions | References

Tables | Figures

◄ | ►

◄ | ►

Back | Close

Full Screen / Esc

Printer-friendly Version

Interactive Discussion

Table 1. Input, parameters, and parameterization method used in the modelling framework.

Group	Symbol	Description	Spatial unit	Values/range	Methods/remarks
Rainfall	R_t	Rainfall flux (m h^{-1})	REW	–	Averaging a precipitation map over each REW for each time step. Precipitation maps have grid cell sizes of 37.5 m^2, and are created by inverse distance interpolation of observed precipitation using an inverse distance exponent of two (Ahrens, 2006).
	R_{avg}	Event averaged rainfall intensity (m h^{-1})	REW	–	Calculated for the period that averaged rain depth over the REWs is above 0.07 mm. This threshold is arbitrarily set to indicate the smallest rain depth that is recognized as an event.
	T	Event duration (h)	REW	–	Sum of time steps that the averaged rain depth over the REWs is above 0.07 mm
Climate	$\overline{T_m}$	Monthly averaged Temperature (˚C)	Catchment	–	Measured in 0.5 h intervals and averaged on a monthly basis
	l_d	Monthly average day length (h)	Catchment	–	Sum of the daylight hours, estimated using the CBM model (Forsythe et al., 1995) over each month
Vegetation	LAI	Leaf area index (–)	REW	0.01–10	Estimated for each vegetation unit using the LAI global dataset (Scurlock et al., 2001). A surcharge of 2 was added to the forest-type units to compensate for the vegetation layer at the forest floor (Breuer et al., 2003). The average LAI for each vegetation unit was obtained by reducing the estimated LAI with a fraction of vegetation cover observed in the field.
	v_{cov}	Fraction of vegetation cover (–)	REW	0.05–1	Field observation. Note that the vegetation cover fraction observed in the field was only used for deriving the average LAI of the vegetation units. For calculating interception and net rain flux, the vegetation cover fraction at the REWs was estimated using Eq. (11).
	$S_{I,leaf}$	Maximum interception capacity per LAI (mm)	REW	0.001–1.3	Estimated for each vegetation type using values suggested by Koivusalo et al. (2006) and Brolsma et al. (2010). A surcharge of 0.3 mm was added to the forest-type units to account for the additional interception capacity of the undergrowth at the forest floor.
	k	Light extinction coefficient (–)	Catchment	0.5	Brolsma et al. (2010); Kuriakose et al. (2009)
Soil	K_s	Saturated hydraulic conductivity (m h^{-1})	REW	–	Estimated from the REW's regolith properties, which are related to the geomorphology. The referred-to values are reported in Rawls et al. (1982). See Table 2.
	H_f	Matric suction at the wetting front (m)	REW	–	Estimated from the REW's regolith properties, which are related to the geomorphology. The referred-to values are reported in Rawls et al. (1982). See Table 2.
	η	Porosity (–)	Catchment	0.42	Used value for the loamy soil, which is the average soil texture of the catchment (Rawls et al., 1982).
	θ	Moisture content at the start of simulation period (–)	Catchment	0.25	We used a slightly smaller value for the moisture content at field capacity for loamy soil (i.e. the average soil texture of the catchment) as the catchment was relatively dry at the start of the simulation period.
	θ_{PWP}	Moisture content at wilting point (–)	Catchment	0.1	Value used for loamy soil, which is the average soil texture of the catchment (Rawls et al., 1982).
	θ_{fc}	Moisture content at Field capacity (–)	Catchment	0.27	Value used for loamy soil, which is the average soil texture of the catchment (Rawls et al., 1982).
	k_θ^*	Critical moisture content (–)	Catchment	0.5	Dingman (2002) and Gervais et al. (2012)
	r	Root zone depth (cm)	Catchment	50	Assumed
	c_1	Micro relief on REW surface (mm)	REW	80–0.4	Generated random fields of micro relief, using different values of c_1 in a circular variogram model, for a hypothetical hill slope that has the same slope gradient for each REW. We determined the drainage direction path over the REWs by following the direction from a cell to the steepest descent as determined by its eight neighbouring cells (Burrough and McDonnell, 2004). Chose the c_1 value that results in a flow pattern most resembling that of the REW observed in the field.

Table 1. Continued.

Group	Symbol	Description	Spatial unit	Values/range	Methods/remarks
REW Geometry	s	Slope gradient ($m\,m^{-1}$)	REW	–	Extracted from the digital elevation data (DEM)
	L	Unit Length (m)	REW	–	Calculated as a weighted average of the longest drainage paths from the REW's divide to the REW's outlets according to the upstream areas.
Channel	A_r	Channel cross section (m^2)	Sub-catchment	0.3 (L) 0.15 (M) 0.04 (S)	Field observation at a number of transects along stream channels. We calculated the average cross section for each sub-catchment.
	D_i	Distance from a REW outlet to the (sub) catchment outlet	REW	–	Calculated from the local drainage direction (ldd) map
	S_i	Channel slope ($m\,m^{-1}$)	REW	–	Averaged slope at each grid cell over the drainage path from a REW outlet to the (sub)catchment outlet.
	n	Manning's coefficient ($h\,m^{-1/3}$)	Catchment	0.3	These estimations are based on the observed stream bed materials, using a value given in Chow et al. (1988)

Table 2. Soil texture and corresponding soil hydraulic parameters (K_s and H_f) estimated for each type of geomorphologic unit (Rawls et al., 1982).

Geomorphologic unit	Soil/regolith type	K_s (mm h^{-1})	H_f (m)
Hogback	outcrops	0.01	-10^{-5}
River plain	sandy clay loam	4.3	-0.449
Alluvial fan (coarse regolith)	sandy clay loam	4.3	-0.449
Alluvial fan (fine regolith)	clay loam	2.3	-0.446
Colluvium	clay loam	2.3	-0.446
Active badlands	black marls	0.6	-0.714
Inactive badlands	silt clay	0.9	-0.647
Glacis	slit loam	6.8	-0.404
Glacis remnant	silt loam	6.8	-0.404
Mass movement	loamy sand	61.1	-0.142
Debris slope	loamy sand	61.1	-0.142

Discussion Paper | Discussion Paper | Discussion Paper | Discussion Paper |

HESSD

10, 1769–1817, 2013

Hortonian overland flow closure relations

E. Vannametee et al.

Title Page

Abstract | Introduction

Conclusions | References

Tables | Figures

◄ | ►

◄ | ►

Back | Close

Full Screen / Esc

Printer-friendly Version

Interactive Discussion

Table 3. Characteristics of REWs for catchments.

Catchment	N	Area (10^3 m^2)		s (m m−1)		L (m)	
		max	min	max	min	max	min
L	44	1140	21	0.74	0.03	1737	76
M	12	776	27	0.61	0.09	1501	196
S	3	288	53	0.38	0.18	1035	307

N = number of REWs; s = slope (m m^{-1}); L = length (m).

Table 4. Characteristics of the rainstorm events selected for evaluation of closure relations.

Catchment	N	R_{avg} (mm h^{-1})				T (h)				Runoff coefficient (–)			
		min	med	max	S.D.	min	med	max	S.D.	min	med	max	S.D.
L	15	2.0	4.5	34.6	10.4	0.4	4.3	27.9	7.9	0.02	0.04	0.11	0.03
M	7	4.0	5.1	8.0	1.8	3.6	5.5	9.4	8.0	0.017	0.04	0.13	0.04
S	17	2.0	4.1	29.3	7.7	0.4	3.9	23.5	6.9	0.015	0.08	0.3	0.09

R_{avg} = average rainfall intensity (mm h^{-1}); T = event duration (h); N = number of events; med = median; S.D. = standard deviation.

Table 5. Performance of C and C^* without calibration.

Catchment	N	Closure relation	E				$e_{Q_{cum}}$			
			min	med	max	S.D.	min	med	max	S.D.
L	15	C	−115.5	−2.6	0.78	35.6	54.2	205.6	879.9	233.9
		C^*	−983.6	−40.3	−3.6	264.5	50.8	277.0	1271.0	311.8
M	7	C	−292.0	−8.2	0.64	107.2	32.2	197.6	1462.0	506.3
		C^*	−875.2	−23. 8	−3.2	327.6	35.0	238.2	1565.0	545.4
S	17	C	−84.5	0.5	0.84	25.6	12.2	36.9	781.7	244.1
		C^*	−2573.0	−6.9	0.24	619.9	10.0	101.0	1378.0	359.7
Total	39	C	−292.0	−0.9	0.84	52.6	12.2	136.0	1462.0	306.9
		C^*	−2573.0	−19.2	0.24	452.7	10.0	176.8	1565.0	378.7

N = number of events; E = Nash-Sutcliffe index; $e_{Q_{cum}}$ = percent error in total discharge volume, med = median; S.D. = standard deviation.

Table 6. Statistics of the calibration and validation events.

Catchment	Event type	N	R_{avg} (mm h^{-1})				T (h)				Runoff coefficient (–)			
			min	med	max	S.D.	min	med	max	S.D.	min	med	max	S.D.
L	calibration	7	2.0	3.2	34.6	11.9	0.4	4.5	8.7	2.9	0.02	0.03	0.05	0.01
	validation	8	2.0	5.5	30.4	9.7	0.7	3.5	27.9	10.5	0.02	0.05	0.11	0.03
M	calibration	4	4.2	4.7	7.4	1.5	3.6	5.1	7.3	1.6	0.02	0.04	0.05	0.16
	validation	3	4.0	7.3	8.0	2.2	3.8	11.4	26	11.3	0.03	0.08	0.13	0.52
S	calibration	8	2.4	3.8	29.3	9.9	0.4	4.3	8.9	3.0	0.04	0.07	0.14	0.04
	validation	9	2.0	4.2	19.4	5.3	0.8	3.8	23.5	8.9	0.02	0.13	0.3	0.11

R_{avg} = average rainfall intensity (m h^{-1}); T = event duration (h); N = numbers of events; med = median; S.D. = standard deviation.

Hortonian overland flow closure relations

E. Vannametee et al.

Table 7. Performance of non-calibrated closure relations evaluated for calibration and validation events.

| Catchment | Event types | E | | | | $e_{Q_{cum}}$ | | | |
| | | C | | C^* | | C | | C^* | |
		med	S.D.	med	S.D.	med	S.D.	med	S.D.
L	calibration	−6.5	41.4	−72.2	172.0	256.4	186.2	277.0	200.5
	validation	−0.9	30.6	−25.7	338. 5	111.8	276.3	237.3	399.6
M	calibration	−23.1	138.3	−193.5	402.4	438.4	608.7	524.5	658.4
	validation	−3.7	4.6	−19.2	14.4	144.0	99.4	229.4	116.4
S	calibration	0.35	20.8	−12.4	85.6	83.3	221.0	138.2	244.4
	validation	0.52	30.1	−2.9	854.3	29.9	276.5	64.1	441.2

N = number of events; med = median; S.D. = standard deviation ; E = Nash-Sutcliffe index; $e_{Q_{cum}}$ = percent error in total discharge volume.

Table 8. Performance of C and C^* after calibration.

Catchment	N	Closure relations	E				$e_{Q_{cum}}$			
			min	med	max	S.D.	min	med	max	S.D.
L	8	C	−1.2	0.32	0.81	0.6	14.3	48.2	132.0	36.7
		C^*	−0.6	−0.4	0.07	0.2	74.3	84.6	96.4	8.5
M	3	C	−0.7	0.36	0.44	0.6	55.3	63.4	68.5	6.7
		C^*	−0.5	−0.36	−0.3	0.2	72.9	92.6	95.8	12.4
S	9	C	−16.3	0.13	0.86	6.5	11.8	72.9	308.2	103.9
		C^*	−165.6	−0.3	−0.03	55	49.6	88.2	191.7	41.5
Total	20	C	−16.3	0.3	0.86	4.5	11.8	60.7	308.2	72.3
		C^*	−165.6	−0.35	0.07	36.9	49.6	87.5	191.7	27.8

N = number of events; E = Nash-Sutcliffe index; $e_{Q_{cum}}$ = percent error in total discharge volume, med = median; S.D. = standard deviation.
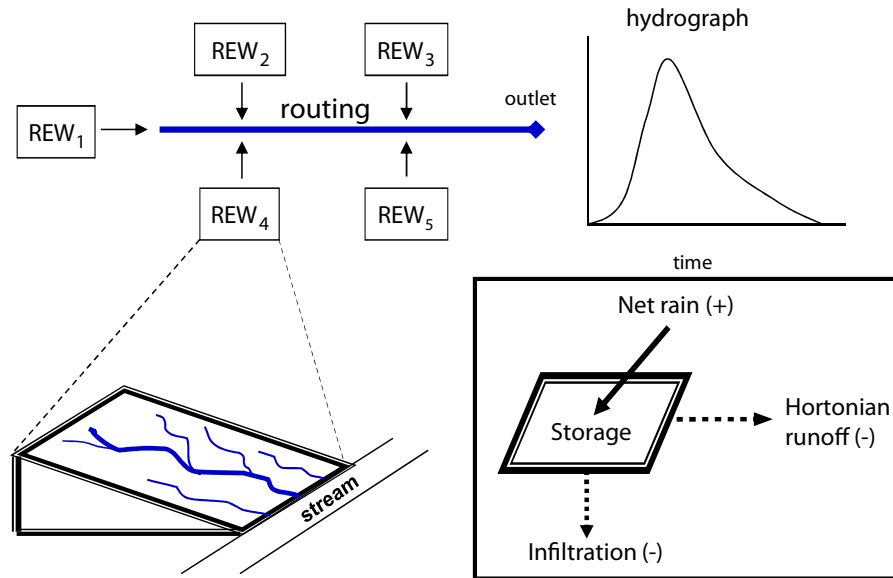
Fig. 1. Schematic representation of the modelling framework used in the study. The Hortonian runoff generating processes for individual REWs defined in the closure relation are shown in concept in the box. The plus and minus signs indicate incoming and outgoing fluxes of the REWs, respectively.
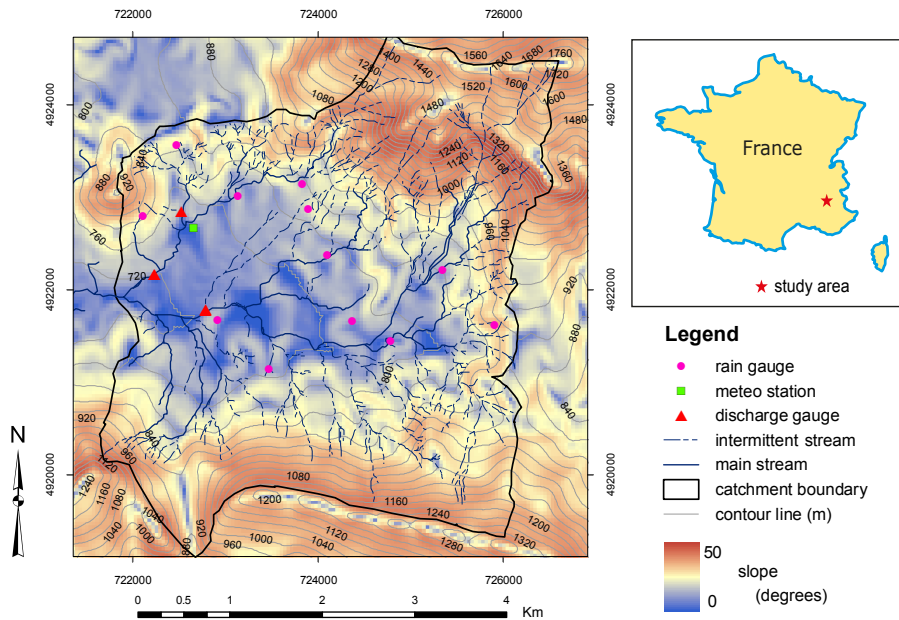
Fig. 2. Location and topographical characteristics of the study catchment, including the measurement locations of rainfall, meteo, and discharge data.

Legend

- rain gauge
- meteo station
- discharge gauge
- intermittent stream
- main stream
- catchment boundary
- contour line (m)

slope (degrees)

★ study area

France
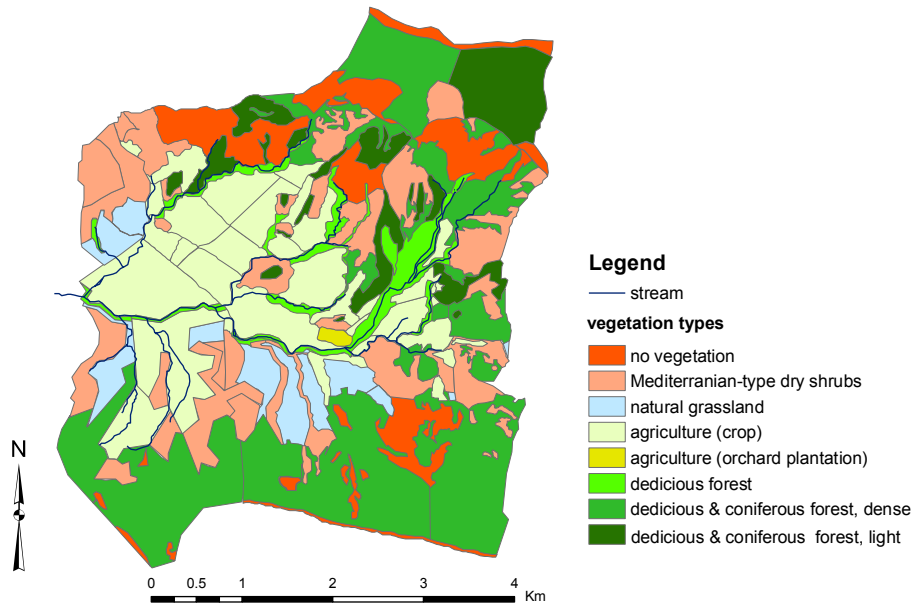
Fig. 3. Vegetation characteristics of the catchment.

Legend

— stream

vegetation types

- no vegetation
- Mediterranian-type dry shrubs
- natural grassland
- agriculture (crop)
- agriculture (orchard plantation)
- dedicious forest
- dedicious & coniferous forest, dense
- dedicious & coniferous forest, light

N

0 0.5 1 2 3 4 Km

Title Page

Abstract | Introduction

Conclusions | References

Tables | Figures

◀ | ▶|

◀ | ▶

Back | Close

Full Screen / Esc

Printer-friendly Version

Interactive Discussion

Legend

Hydrology
- ▲ discharge gauge
- — stream

Sub-catchment and REW
- L
- M
- S
- REW boundary

Geomorphology
- hogback
- river plain
- alluvial fan (coarse regolith)
- alluvial fan (fine regolith)
- colluvium
- active badlands
- inactive badlands
- glacis
- glacis remnant
- mass movement
- debris (scree) slope

Fig. 4. Geomorphology and REWs of the catchment.

Title Page

Abstract | Introduction

Conclusions | References

Tables | Figures

|◄ | ►|

◄ | ►

Back | Close

Full Screen / Esc

Printer-friendly Version

Interactive Discussion
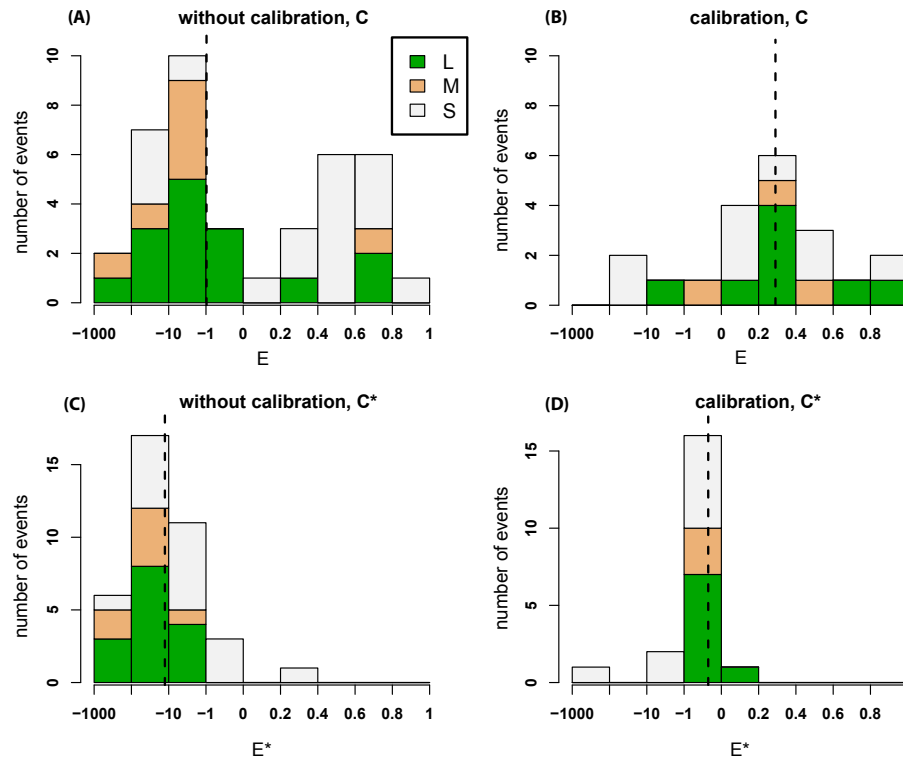
Fig. 5. Nash-Sutcliffe index (E^*) in the L, M and S catchment calculated for the closure relations C (top panels, **A** and **B**) and C^* (bottom panels, **C** and **D**). Left panels, without calibration; right panels, with calibration. Vertical dashed lines indicate the median of the Nash-Sutcliffe index. Note that plots on the right panel show the evaluation only with the validation events.
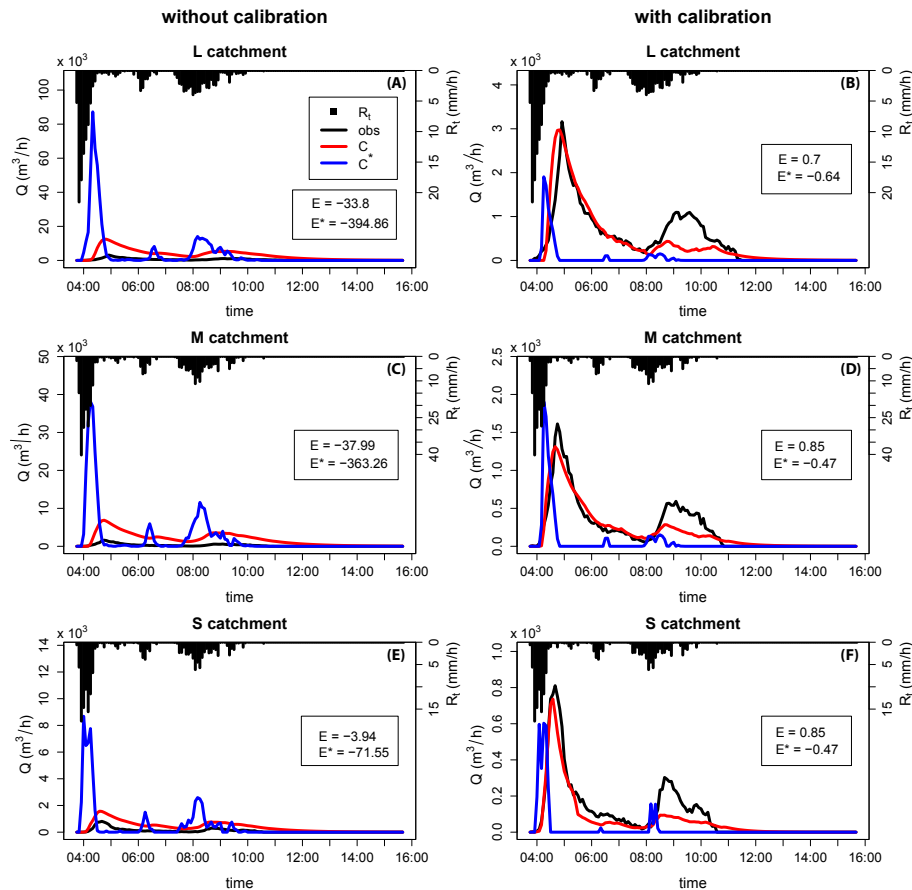
Fig. 6. Hydrographs (Q, $m^3\,h^{-1}$) modelled using the closure relation C (red) and C^* (blue) and observed (obs, black), for an event on 17 June 2010. Rainfall intensity (R_t, $mm\,h^{-1}$) is shown on the secondary axis. E and E^* are the Nash-Sutcliffe indexes for the closure relation C and C^*, respectively. Left (**A**, **C**, **E**) panels, without calibration; right panels (**B**, **D**, **F**), with calibration.
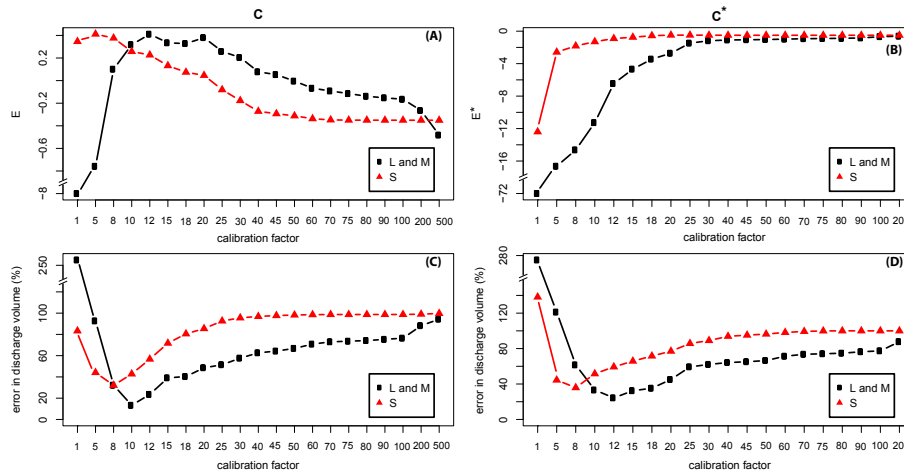
Fig. 7. Median of the Nash-Sutcliffe index, E (**A** and **B**), and discharge volume error as a percentage (**C** and **D**) calculated from events used for calibration (y-axis) as a result of different calibration factors (x-axis) for L and M catchments together (black line, rectangular dots), and S catchment (red lines, triangle dots) for the closure relation C and C^*.
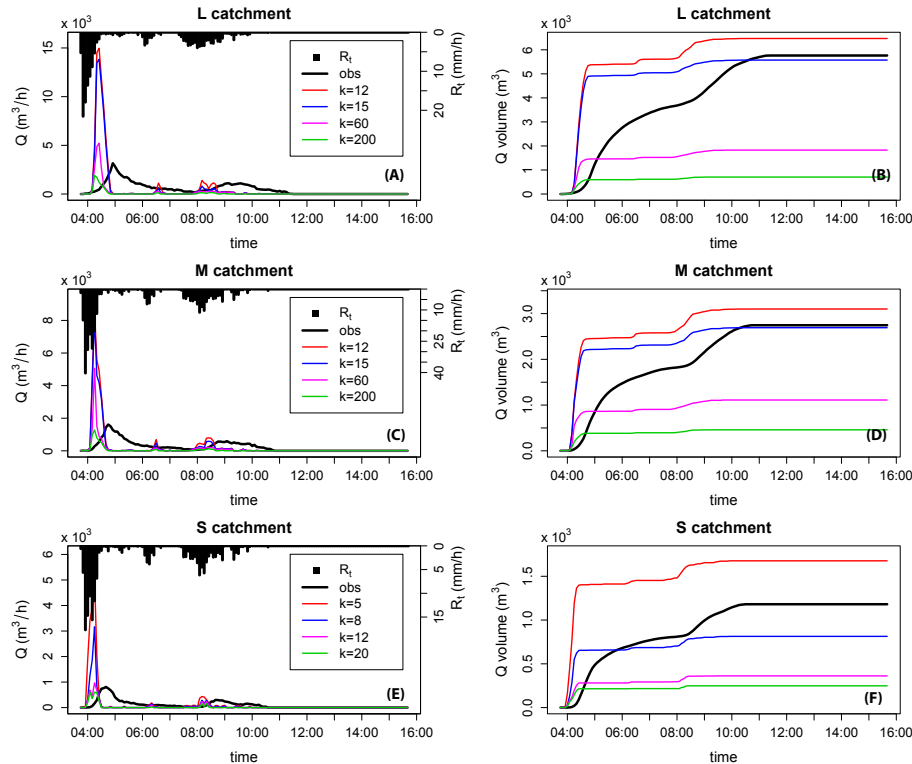
Fig. 8. Hydrographs ($m^3 h^{-1}$, left panel: **A**, **C**, **E**) and the corresponding cumulative discharge volume (m^3, right panel: **B**, **D**, **F**) from individual catchments simulated using the closure relation C^* with different calibration factors, k, for the event observed on 17 June 2010. Rainfall intensity (R_t, $mm h^{-1}$) is plotted on the secondary axis.
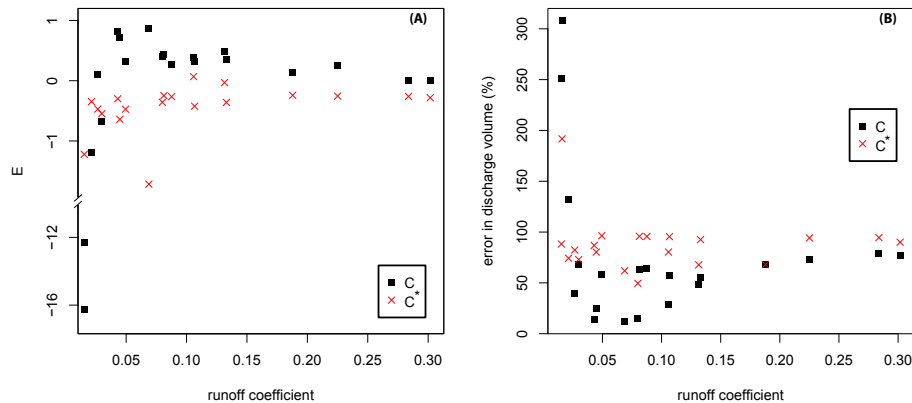
Fig. 9. Performance of the calibrated closure relation C and C^* versus the runoff coefficient of events. **(A)** Nash-Sutcliffe index; **(B)** percent error in discharge volume.